Constructing Hopf Insulator from Geometric Perspective of Hopf Invariant

Zhi-Wen Chang(常治文)[1], Wei-Chang Hao(郝维昌)[2], Miguel Bustamante[3], and Xin Liu(刘鑫)[1*]

[1]*Institute of Theoretical Physics, School of Physics and Optoelectronic Engineering, Beijing University of Technology, Beijing 100124, China*
[2]*School of Physics, Beihang University, Beijing 100191, China*
[3]*Complex and Adaptive Systems Laboratory, School of Mathematics and Statistics, University College Dublin, Belfield, 4, Dublin, Ireland*

(Received 17 November 2023; accepted manuscript online 26 February 2024)

We propose a method to construct Hopf insulators based on the study of topological defects from the geometric perspective of Hopf invariant I. Firstly, we prove two types of topological defects naturally inhering in the inner differential structure of the Hopf mapping. One type is the four-dimensional point defects, which lead to a topological phase transition occurring at the Dirac points. The other type is the three-dimensional merons, whose topological charges give the evaluations of I. Then, we show two ways to establish the Hopf insulator models. One approach is to modify the locations of merons, thereby the contributions of charges to I will change. The other is related to the number of defects. It is found that I will decrease if the number reduces, while increase if additional defects are added. The method developed in this study is expected to provide a new perspective for understanding the topological invariants, which opens a new door in exploring and designing novel topological materials in three dimensions.

DOI: 10.1088/0256-307X/41/3/037302

A topological material demonstrating new states of quantum matter has a bulk-boundary correspondence, i.e., the bulk possesses energy bands that carry non-vanishing topological invariants, in correspondence to the emergence of singular states on its boundaries. The three-dimensional (3D) Hopf insulator studied in this paper is a typical example:[1–4] a fully opened band gap exists in the insulating bulk, while the energy bands carry non-zero Hopf invariants, which naturally arouses gap-closed conducting states on the surfaces.

We have proved that for a two-dimensional (2D) insulator, its invariant, the Chern number,[5,6] can be obtained through the differential structures of two types of topological defects arising from a two-band model: the 3D monopoles and 2D merons, as shown in Refs. [7,8]. We attempt to generalize the method to 3D Hopf insulator, whose topological invariant is the Hopf invariant.[9–14] Furthermore, we introduce two ways to construct Hopf insulator models based on the method.

A Hopf insulator is a special class of 3D topological insulator that exists outside the conventional tenfold-way classification.[15,16] Up to date, such a structure has been only realized in a 3D circuit[17] and simulated in a single-qubit quantum simulator.[18] The main difficulties for realizing Hopf insulators are the demands of having exactly two bands together with the long-range spin-orbit coupling, which are unable to exist simultaneously in many materials. Therefore, designing new Hopf insulator models is helpful for searching experimental materials.

In this Letter, from the geometric viewpoint of the Hopf mapping, we find out two types of topological defects: the four-dimensional (4D) point defects and the 3D merons. We test the method by computing the Hopf invariants of a typical example. We propose two ways to establish new Hopf insulator models. Several examples with non-zero Hopf invariants are presented.

Topological Defects and Hopf Invariant. We will show the connection between the topological defects and the Hopf insulator in terms of a typical model.

A Hopf insulator is a 3D topological insulator that exhibits an insulating bulk state, with the energy bands carrying a non-vanishing topological number, i.e., the Hopf invariant, computed as[19–21]

$$I = \frac{1}{2\pi^2}\int \epsilon^{abcd}\hat{n}_a\partial_{k_x}\hat{n}_b\partial_{k_y}\hat{n}_c\partial_{k_z}\hat{n}_d d^3k, \tag{1}$$

where $a, b, c, d = 1, 2, 3, 4$; $\boldsymbol{n} = (n_1, n_2, n_3, n_4)$ is a 4D vector, $\boldsymbol{n} = \boldsymbol{n}(k_x, k_y, k_z)$. The induced unit vector $\hat{\boldsymbol{n}} = \frac{\boldsymbol{n}}{|\boldsymbol{n}|} = (\hat{n}_1, \hat{n}_2, \hat{n}_3, \hat{n}_4)$ forms a unit 3-sphere S^3, i.e., $\hat{n}_1^2+\hat{n}_2^2+\hat{n}_3^2+\hat{n}_4^2 = 1$. On the other hand, the Brillouin zone forms a T^3 due to the periodicity of the momentum components, $k_x, k_y, k_z \in [-\pi, \pi)$. Mathematically $\hat{\boldsymbol{n}}$ gives a map, $\hat{\boldsymbol{n}} : T^3 \to S^3$.

Rewriting $\boldsymbol{n}$ as a two-component spinor $z = (z_1, z_2)^T$, where $z_1 = n_1 + \mathrm{i}n_2$, $z_2 = n_3 + \mathrm{i}n_4$, one can define a 3D Hamiltonian vector employed in a two-band model, $\boldsymbol{h} = (h_x, h_y, h_z)$, where $h_i = z^\dagger\sigma_i z$, $i = x, y, z$, with σ_i, $i = x, y, z$ being the Pauli matrices. The corresponding unit vector $\hat{\boldsymbol{h}} = \frac{\boldsymbol{h}}{|\boldsymbol{h}|}$ forms a 2-sphere S^2, playing the role of a Hopf map, $\hat{\boldsymbol{h}} : S^3 \to S^2$. The mapping degree is denoted as I.

It can be proved that the eigenvalues of such a two-band model are $E_\pm = \pm|\boldsymbol{h}| = \pm|\boldsymbol{n}| = \pm\sqrt{n_1^2+n_2^2+n_3^2+n_4^2}$, leading to a band gap $\Delta E = 2|\boldsymbol{n}|$.

*Corresponding author. Email: xin.liu@bjut.edu.cn
© 2024 Chinese Physical Society and IOP Publishing Ltd

The gap closing-up condition $\Delta E = 0$ is reached when $n_1 = n_2 = n_3 = n_4 = 0$.

Considering a concrete model:[12–14]

$$\begin{aligned} &n_1 = \sin k_x, \quad n_2 = \sin k_y, \quad n_3 = \sin k_z, \\ &n_4 = \cos k_x + \cos k_y + \cos k_z - m, \end{aligned} \tag{2}$$

one has the Hopf invariant[12,14,20]

$$I = \begin{cases} 0, & |m| > 3, \\ -1, & 1 < |m| < 3, \\ +2, & -1 < |m| < 1. \end{cases} \tag{3}$$

In the following, we will show that the Hopf invariant I can be obtained through an analysis of the singular points residing in S^3.

Four-Dimensional Point Defects. The integrand of Eq. (1) carries a geometric meaning, the solid angle of S^3; its integral gives $2\pi^2$, the surface area of S^3, that is, $\int_{S^3} \epsilon^{abcd}\hat{n}_a\partial_{k_x}\hat{n}_b\partial_{k_y}\hat{n}_c\partial_{k_z}\hat{n}_d d^3k = 2\pi^2$. The pull-back of this equation gives the $\hat{\boldsymbol{n}}$-mapping degree, i.e., the Hopf invariant I,

$$I = \frac{1}{2\pi^2}\int_{\hat{\boldsymbol{n}}^*(S^3)} \epsilon^{abcd}\hat{n}_a\partial_{k_x}\hat{n}_b\partial_{k_y}\hat{n}_c\partial_{k_z}\hat{n}_d d^3k, \tag{4}$$

where $\hat{\boldsymbol{n}}^*(S^3) = T^3$ indicates that the pull-back of S^3 is the Brillouin zone T^3. Given that S^3 is a closed boundary, $S^3 = \partial B^4$, where B^4 is a solid 4-ball, the integral on S^3 can be turned to a body integral over B^4 in the light of the Stokes theorem,

$$I = \frac{1}{2\pi^2}\int_{B^4} \frac{1}{4!}\epsilon^{abcd}\epsilon^{\mu\nu\rho\eta}\partial_\mu\hat{n}_a\partial_\nu\hat{n}_b\partial_\rho\hat{n}_c\partial_\eta\hat{n}_d d^4k, \tag{5}$$

where a topological scalar current is defined as $j = \frac{1}{2\pi^2}\frac{1}{4!}\epsilon^{abcd}\epsilon^{\mu\nu\rho\eta}\partial_\mu\hat{n}_a\partial_\nu\hat{n}_b\partial_\rho\hat{n}_c\partial_\eta\hat{n}_d$, which is able to be presented in a δ-function form[22]

$$j = \delta^4(\boldsymbol{n})D\Big(\frac{n}{k}\Big), \tag{6}$$

where $D(\frac{n}{k}) = \frac{1}{4!}\epsilon^{abcd}\epsilon^{\mu\nu\rho\eta}\partial_\mu n_a\partial_\nu n_b\partial_\rho n_c\partial_\eta n_d$ is a Jacobian.

The δ-function does not vanish only at the locations $\boldsymbol{n} = 0$, to wit, $n_1 = n_2 = n_3 = n_4 = 0$, implying the existence of a 4D point defect at the center of S^3. Under the regular condition $D(\frac{n}{k}) \neq 0$, $\boldsymbol{n} = 0$ has isolate solutions, in correspondence to the topological defects in a 4D physical momentum space.

On the other hand, however, the pull-back of Eq. (4) is inconsistent with the dimension of the base manifold T^3, as the latter lacks a fourth coordinate beyond k_x, k_y, and k_z. It gives rise to indeterminate evaluation of the Hopf invariant I; namely, a physical topological transition happens at the gap-closing Dirac point, over which I experiences a jump in evaluation.

As far as the concrete model (2) is concerned, the solutions of $\boldsymbol{n} = 0$ yield 4D point defects:

- $(k_x, k_y, k_z) = (0, 0, 0)$, with $m = 3$;
- $(k_x, k_y, k_z) = (0, 0, \pi)$, $(0, \pi, 0)$ and $(\pi, 0, 0)$, with $m = 1$;
- $(k_x, k_y, k_z) = (0, \pi, \pi)$, $(\pi, 0, \pi)$ and $(\pi, \pi, 0)$, with $m = -1$;
- $(k_x, k_y, k_z) = (\pi, \pi, \pi)$, with $m = -3$.

The Hopf invariant I encounters a jump at such a point owing to the singularity of the integral (4), leading to the occurrence of a physical topological transition at a Dirac point.

Merons as 3D Point Defects. The above 4D point defects arise from the spherical center of the S^3; in contrast, merons, i.e., 3D point defects, arise from the respective poles of the north- and south-hemispheres.

The surface of S^3 is topologically non-trivial, having two 3D hemispherical covers diffeomorphic to two 3D Euclidean spaces $\mathbb{R}^3$, respectively. Correspondingly, the Hopf invariant is given as two separate copies,

$$I_{\rm N} = \frac{1}{\pi^2}\int_{T^3_{\rm N}} \epsilon^{abcd}\hat{n}_a\partial_{k_x}\hat{n}_b\partial_{k_y}\hat{n}_c\partial_{k_z}\hat{n}_d d^3k, \tag{7}$$

$$I_{\rm S} = \frac{1}{\pi^2}\int_{T^3_{\rm S}} \epsilon^{abcd}\hat{n}_a\partial_{k_x}\hat{n}_b\partial_{k_y}\hat{n}_c\partial_{k_z}\hat{n}_d d^3k, \tag{8}$$

where π^2 is the area of a half-sphere, $T^3_{\rm N} = \hat{\boldsymbol{N}}^*(S^3_{\rm N})$ and $T^3_{\rm S} = \hat{\boldsymbol{N}}^*(S^3_{\rm S})$ are the pull-backs of the north- and south-hemispheres to the Brillouin zone T^3, respectively.

It should be addressed that $I_{\rm N}$ and $I_{\rm S}$ are not additive. Indeed, the two separate hemispherical covers of S^3 cannot be trivially stuck to each other; otherwise, the additivity inevitably contradicts the topological non-triviality of S^3.

Physically, $I_{\rm N}$ and $I_{\rm S}$ serve as the respective Hopf invariants of the higher and lower energy bands, whose evaluations can be obtained through analysis of the asymptotic behavior of the $\hat{\boldsymbol{n}}$-vector in the respective neighborhoods of the north pole on $S^3_{\rm N}$ and the south pole on $S^3_{\rm S}$.

At north and south poles, the $\hat{\boldsymbol{n}}$ vector is given by $(\hat{n}_1, \hat{n}_2, \hat{n}_3, \hat{n}_4) = (0, 0, 0, 1)$ and $(\hat{n}_1, \hat{n}_2, \hat{n}_3, \hat{n}_4) = (0, 0, 0, -1)$, respectively. In the poles' neighborhoods the asymptotic behavior is individually expressed as $(\hat{n}_1, \hat{n}_2, \hat{n}_3, \hat{n}_4) = (\delta_1, \delta_2, \delta_3, 1 - \delta_4)$ and $(\hat{n}_1, \hat{n}_2, \hat{n}_3, \hat{n}_4) = (\delta_1, \delta_2, \delta_3, -1+\delta_4)$, where δ_1, δ_2, δ_3, δ_4 are positive infinitesimals, $0 < \delta_1, \delta_2, \delta_3, \delta_4 \ll 1$.

Without loss of generality, we first examine the integrand of Eq. (7) in the neighborhoods near the north pole, which can be written into two parts as

$$\begin{aligned} &\epsilon^{abcd}\hat{n}_a\partial_{k_x}\hat{n}_b\partial_{k_y}\hat{n}_c\partial_{k_z}\hat{n}_d \\ &= \frac{1}{3!}\epsilon^{\mu\nu\rho}\epsilon^{4ijk}\hat{n}_4\partial_\mu\hat{n}_i\partial_\nu\hat{n}_j\partial_\rho\hat{n}_k \\ &\quad + \frac{1}{2!}\epsilon^{\mu\nu\rho}\epsilon^{i4jk}\hat{n}_i\partial_\mu\hat{n}_4\partial_\nu\hat{n}_j\partial_\rho\hat{n}_k, \end{aligned} \tag{9}$$

where $i, j, k = 1, 2, 3$. It is seen that only third and forth order terms of δ_1, δ_2, δ_3, δ_4 are contained. Thus, ignoring the forth order terms, the first part of Eq. (9) becomes a topological scalar current, while the second part vanishes because of $\partial_\mu\hat{n}_4 = 0$. That is,

$$\begin{aligned} \epsilon^{abcd}\hat{n}_a\partial_{k_x}\hat{n}_b\partial_{k_y}\hat{n}_c\partial_{k_z}\hat{n}_d &= \frac{1}{3!}\epsilon^{\mu\nu\rho}\epsilon^{ijk}\partial_\mu\hat{n}_i\partial_\nu\hat{n}_j\partial_\rho\hat{n}_k \; d^3k \\ &= \pi^2 j, \end{aligned} \tag{10}$$

where j is a topological scalar current, $j = \frac{1}{6\pi^2}\epsilon^{ijk}\epsilon^{\mu\nu\rho}\partial_\mu\hat{n}_i\partial_\nu\hat{n}_j\partial_\rho\hat{n}_k$.

Now, we can rewrite the Hopf invariant Eq. (7) as

$$I_{\rm N} = \int_{T^3_{\rm N}} j d^3k = \int_{T^3_{\rm N}} \delta^3(\boldsymbol{n}') D\Big(\frac{n'}{k}\Big) d^3k, \qquad (11)$$

where $\delta^3(\boldsymbol{n}')$ is a δ-function,[22] $D(\frac{n'}{k}) = \frac{1}{3!}\epsilon^{ijk}\epsilon^{\mu\nu\rho}\partial_\mu N_i \partial_\nu N_j \partial_\rho N_k$ a Jacobian, and $\boldsymbol{n}' = (n_1, n_2, n_3)$ a 3D vector. The δ-function does not vanish only at $\boldsymbol{n}' = \boldsymbol{0}$, hence it is important to study the zero point equation $n_1 = n_2 = n_3 = 0$. Under the regular condition $D(\frac{n'}{k}) \neq 0$, it has L isolate solutions of singular points, i.e., the meron defects, $k^\mu = k^\mu_l$, with $\mu = x, y, z$ and $l = 1, 2, \ldots, L$. Expanding the δ-function onto the singular points, one has

$$\delta^3(\boldsymbol{n}') = \sum_{l=1}^{L} W_l \delta^3(k^\mu - k^\mu_l), \qquad (12)$$

where $W_l = \beta_l \eta_l$ is the topological charge of the l-th meron, with β_l being the Hopf index (notice: not the Hopf invariant mentioned above) and η_l the Brouwer mapping degree. Substituting Eq. (12) into Eq. (11) we finally obtain

$$I_{\rm N} = \int_{T^3_{\rm N}} \Big[\sum_{l=1}^{L} W_l \delta^3(k^\mu - k^\mu_l) D\Big(\frac{n'}{k}\Big)\Big] d^3k = \sum_{l=1}^{L} W_l. \qquad (13)$$

Equation (13) means that the Hopf invariant $I_{\rm N}$ on the north-hemisphere is a sum of the topological charges of the merons that are the pull-back of the north pole. Physically, $I_{\rm N}$ gives the Hopf invariant of the higher energy band, since the eigenvalue in this case is $E = n_4 > 0$ due to $\hat{n}_4 = 1$.

Similarly, the Hopf invariant $I_{\rm S}$ on the south-hemisphere is a sum of the topological charges of the merons stemming from the pull-back of the south pole. $I_{\rm S}$ gives the Hopf invariant of the lower band, since $E = n_4 < 0$ in this case, $I_{\rm S} = \sum_{l=1}^{L'} W_l$, where L' denotes the number of the merons in the south-hemisphere case.

Now, let us take the concrete model (2) as an example. The locations of the merons are determined by the solutions of $n_1 = n_2 = n_3 = 0$:

- $(k_x, k_y, k_z) = (0, 0, 0)$, with $m \neq 3$;
- $(k_x, k_y, k_z) = (0, 0, \pi), (0, \pi, 0), (\pi, 0, 0)$, with $m \neq 1$;
- $(k_x, k_y, k_z) = (0, \pi, \pi), (\pi, 0, \pi), (\pi, \pi, 0)$, with $m \neq -1$;
- $(k_x, k_y, k_z) = (\pi, \pi, \pi)$, with $m \neq -3$.

For every meron, its energy eigenvalue is $E = n_4 \neq 0$, whose sign changes with varying m. We summarize the contributions of the merons' topological charges to the Hopf invariants $I_{\rm N}$ and $I_{\rm S}$:

- When $m > 3$: $n_4 = \cos k_x + \cos k_y + \cos k_z - m < 0$ always. All merons concentrate in the pull-back of the south pole, hence their topological charges contribute to $I_{\rm S}$ only.
- When $1 < m < 3$:
  - at $(k_x, k_y, k_z) = (0, 0, 0)$, $n_4 = 3 - m > 0$. This meron corresponds to the north pole, hence its charge contributes to $I_{\rm N}$;
  - for other merons, $n_4 < 0$. Hence they correspond to the south pole, with the charges contributing to $I_{\rm S}$ only.
- When $-1 < m < 1$:
  - at $(k_x, k_y, k_z) = (0, 0, 0), (0, 0, \pi), (0, \pi, 0)$ and $(\pi, 0, 0)$, there is $n_4 > 0$. These merons correspond to the north pole, with the charges contributing to $I_{\rm N}$;
  - for other merons, $n_4 < 0$. Hence they correspond to the south pole, with the charges contributing to $I_{\rm S}$.
- When $-3 < m < -1$:
  - at $(k_x, k_y, k_z) = (\pi, \pi, \pi)$, $n_4 = -3 - m < 0$. This meron corresponds to the south pole, with the charge contributing to $I_{\rm S}$;
  - for other merons, $n_4 > 0$. Hence they correspond to the north pole, with the charges contributing to $I_{\rm N}$.
- When $m < -3$: $n_4 = \cos k_x + \cos k_y + \cos k_z - m > 0$ for always. All merons correspond to the north pole, with the charges contributing to $I_{\rm N}$ only.

The above discussions are summarized in Table 1.

Table 1. Locations of 3D meron defects of model (2), and the corresponding contributions of topological charges to $I_{\rm N}$ and $I_{\rm S}$ with respect to varying m.

Locations of merons	m values				
(k_x, k_y, k_z)	$(3, +\infty)$	$(1, 3)$	$(-1, 1)$	$(-3, -1)$	$(-\infty, -3)$
$(0, 0, 0)$	$I_{\rm S}$	$I_{\rm N}$	$I_{\rm N}$	$I_{\rm N}$	$I_{\rm N}$
$(0, 0, \pi)$,$(0, \pi, 0)$,$(\pi, 0, 0)$	$I_{\rm S}$	$I_{\rm S}$	$I_{\rm N}$	$I_{\rm N}$	$I_{\rm N}$
$(0, \pi, \pi)$,$(\pi, 0, \pi)$,$(\pi, \pi, 0)$	$I_{\rm S}$	$I_{\rm S}$	$I_{\rm S}$	$I_{\rm N}$	$I_{\rm N}$
(π, π, π)	$I_{\rm S}$	$I_{\rm S}$	$I_{\rm S}$	$I_{\rm S}$	$I_{\rm N}$

Table 2. Topological charges of 3D meron defects in concrete model (2).

(k_x, k_y, k_z)	$(0, 0, 0)$	$(0, \pi, \pi)$	$(\pi, 0, \pi)$	$(\pi, \pi, 0)$
Topological charge	$+1$	$+1$	$+1$	$+1$
(k_x, k_y, k_z)	(π, π, π)	$(0, 0, \pi)$	$(0, \pi, 0)$	$(\pi, 0, 0)$
Topological charge	-1	-1	-1	-1

Next, we are at the stage to compute the topological charges of the merons. A meron's charge is equal to the index of the 3-vector $\boldsymbol{n}' = (n_1, n_2, n_3)$ in the meron's neighborhood, which can be read out from the distribution of the $\boldsymbol{n}'$-field. The results are summarized in Table 2. To help the readers to achieve a better understanding, we take the meron located at $(k_x, k_y, k_z) = (0, 0, 0)$ as an example

to show the computations of the data in Table 2:

- The index of an n-dimensional vector field around a singular point is defined as $(-1)^k$, where k and $(n-k)$ are the numbers of contracting and expanding dimensions, respectively.
- For the purpose of counting the number of contracting dimensions of $\boldsymbol{n}'$-field around the given meron, we present the projections of the $\boldsymbol{n}'$-field on the $k_z = 0$ and $k_x = 0$ planes, as illustrated in Fig. 1, a plot of $\boldsymbol{n}'$.
- It is seen that, in three directions, the arrows point outwards from the meron, indicating that the number of the contracting dimensions is zero. Hence the topological charge of the meron is $(-1)^0 = +1$.
- Actually, the charges of other merons can also be recognized from Fig. 1. For instance, the left sub-figure shows the vectors converge to the position $(k_x, k_y) = (\pi, 0)$ at k_x direction, while diverge from it at k_y direction; the right sub-figure shows the vector diverge to and converge from $(k_y, k_z) = (0, \pi)$ along k_y and k_z axes, respectively. Consequently, the meron emerging at $(k_x, k_y, k_z) = (\pi, 0, \pi)$ has two contracting dimensions with the charge of $(-1)^2 = +1$.

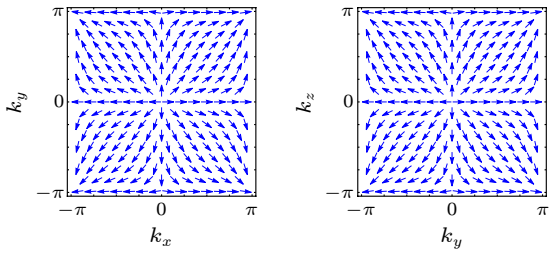

Fig. 1. Projections of 3D vector field $\boldsymbol{n}' = (\sin k_x, \sin k_y, \sin k_z)$ on $k_z = 0$ and $k_x = 0$ planes. Left: on the $k_z = 0$ plane, the arrows pointing outwards from the center $(0, 0, 0)$ in the k_x and k_y directions. Right: on the $k_x = 0$ plane, the arrows pointing outwards from the position in the k_y and k_z directions. Therefore, the arrows pointing outwards from the meron in three directions; namely, the number of contracting dimensions is zero, which leads to the meron's topological charge, $(-1)^0 = +1$. The charges of other merons can be obtained similarly.

Finally, Tables 1 and 2 together give the Hopf invariants $I_{\rm N}$ and $I_{\rm S}$:

- When $m > 3$, all the topological charges of the merons contribute to $I_{\rm S}$ (thus $I_{\rm S} = 0$), and have no contributions to $I_{\rm N}$ (thus $I_{\rm N} = 0$).
- When $1 < m < 3$, only the topological charge of the meron located at $(k_x, k_y, k_z) = (0, 0, 0)$ has a contribution to $I_{\rm N}$; all the others contribute to $I_{\rm S}$. Thus, $I_{\rm N} = +1$, $I_{\rm S} = -1$.
- When $-1 < m < 1$, the topological charges of the merons located at $(k_x, k_y, k_z) = (0, 0, 0)$, $(0, 0, \pi)$, $(0, \pi, 0)$, and $(\pi, 0, 0)$ have contributions to $I_{\rm N}$; all the others contribute to $I_{\rm S}$. Thus, $I_{\rm N} = -2$, $I_{\rm S} = +2$.
- When $-3 < m < -1$, only the topological charge of the meron located at $(k_x, k_y, k_z) = (\pi, \pi, \pi)$ has a contribution to $I_{\rm S}$; all the others contribute to $I_{\rm N}$. Thus, $I_{\rm N} = +1$, $I_{\rm S} = -1$.
- When $m < -3$, all the topological charges of the merons contribute to $I_{\rm N}$ (thus $I_{\rm N} = 0$), and have no contributions to $I_{\rm S}$ (thus $I_{\rm S} = 0$).

In summary,

$$I_{\rm N} = \begin{cases} 0, & m > 3, \\ +1, & 1 < m < 3, \\ -2, & -1 < m < 1, \\ +1, & -3 < m < -1, \\ 0, & m < -3; \end{cases}$$
$$I_{\rm S} = \begin{cases} 0, & m > 3, \\ -1, & 1 < m < 3, \\ +2, & -1 < m < 1, \\ -1, & -3 < m < -1, \\ 0, & m < -3. \end{cases} \tag{14}$$

In Eq. (14) it is recognized that the Hopf invariant of the lower band, $I_{\rm S}$, exactly reproduces the I-evaluation of Eq. (3).

Constructing Hopf Insulator Model. Now, we present two ways to establish the Hopf insulator from the studied model (2). It is noticed that we only discuss the meron defects for the reason that their charges determine the values of Hopf invariant I.

One approach is to alter the contribution of merons by modifying the n_4 term. Here, we propose the following example:

$$n_1 = \sin k_x, \quad n_2 = \sin k_y, \quad n_3 = \sin k_z,$$
$$n_4 = \cos k_x \cos k_y + \cos k_z - m. \tag{15}$$

Since n_1, n_2, and n_3 are intact, the locations of topological defects are the same as the model (2). Therefore, to compute the Hopf invariants of the two bands, we only need to analyze the positions of the merons according to the sings of n_4, as presented in Table 3.

Table 3. Locations of 3D meron defects of model (15), and the corresponding contributions of topological charges to $I_{\rm N}$ and $I_{\rm S}$ with respect to varying m.

Locations of merons	m values			
(k_x, k_y, k_z)	$(2, +\infty)$	$(0, 2)$	$(-2, 0)$	$(-\infty, -2)$
$(0, 0, 0)$, $(\pi, \pi, 0)$	$I_{\rm S}$	$I_{\rm N}$	$I_{\rm N}$	$I_{\rm N}$
$(0, \pi, \pi)$,$(\pi, 0, \pi)$	$I_{\rm S}$	$I_{\rm S}$	$I_{\rm S}$	$I_{\rm N}$
(π, π, π),$(0, 0, \pi)$,$(0, \pi, 0)$, $(\pi, 0, 0)$	$I_{\rm S}$	$I_{\rm S}$	$I_{\rm N}$	$I_{\rm N}$

From Table 2, we obtain

$$I_{\rm N}=\begin{cases}0, & m>2,\\ +2, & 0<m<2,\\ -2, & -2<m<0,\\ 0, & m<-2;\end{cases}$$
$$I_{\rm S}=\begin{cases}0, & m>2,\\ -2, & 0<m<2,\\ +2, & -2<m<0,\\ 0, & m<-3.\end{cases} \tag{16}$$

The other approach to construct the Hopf insulator model relies on the number of the merons. In this approach, we acquire an experiential conclusion: the Hopf invariant I would decrease if we reduce the number of defects, while I would increase if we add additional defects. To demonstrate this, we first consider the following example:

$$n_1=\sin\frac{k_x}{2},\quad n_2=\sin\frac{k_y}{2},\quad n_3=\sin k_z,$$
$$n_4=\cos k_x+\cos k_y+\cos k_z-m. \tag{17}$$

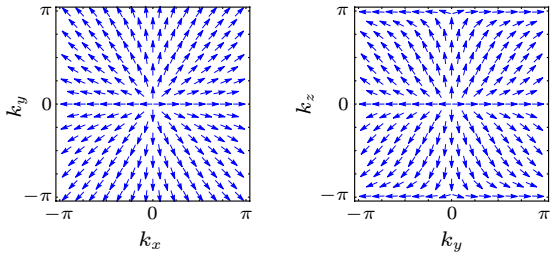

Fig. 2. Projections of 3D vector field $\boldsymbol{n}'=(\sin\frac{k_x}{2},\sin\frac{k_y}{2},\sin k_z)$ around singular point $(k_x,k_y,k_z)=(0,0,0)$ on $k_z=0$ and $k_x=0$ planes. It is recognized that only two singular points exist in this vector field.

Clearly, the model possesses only two merons located at $(k_x,k_y,k_z)=(0,0,0)$ and $(0,0,\pi)$, which are also able to be found out from the configuration of the 3D vector $\boldsymbol{n}'=(n_1,n_2,n_3)$, as illustrated in Fig. 2. The former forms a source point, namely, having three expanding dimensions, while the latter has one contracting (k_z direction). As a consequence, their charges are $(-1)^0=+1$ and $(-1)^1=-1$, respectively.

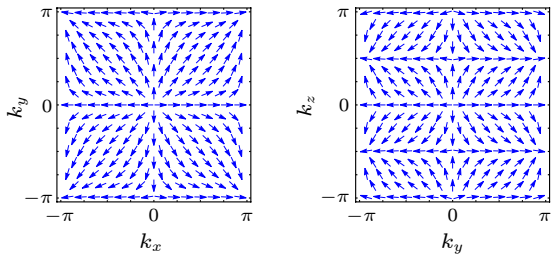

Fig. 3. Projections of 3D vector field $\boldsymbol{n}'=[\sin k_x,\sin k_y,\sin(2k_z)]$ around the singular point $(k_x,k_y,k_z)=(0,0,0)$ on $k_z=0$ and $k_x=0$ planes. One can discover eight additional merons that are distinct from the initial positions in model (2).

In this model, the non-vanishing Hopf invariants appear only when $1<m<3$. The charge of the meron $(0,0,0)$ contributes to $I_{\rm N}$ owing to $n_4>0$, while the other one contributes to $I_{\rm S}$ because of $n_4<0$. Hence, $I_{\rm N}=+1$, $I_{\rm S}=-1$. For all other ranges of m, one can easily find $I_{\rm N}=I_{\rm S}=0$. Compared with the Hopf invariant of model (2), i.e., Eq. (14), the case of $|I|=2$ disappears.

Now, we turn to considering the other situation, that is, increasing the number of merons. The model is taken as

$$n_1=\sin k_x,\quad n_2=\sin k_y,\quad n_3=\sin(2k_z),$$
$$n_4=\cos k_x+\cos k_y+\cos k_z-m. \tag{18}$$

The locations of defects and their charges can be read out from the configuration of the 3D vector $\boldsymbol{n}'=[\sin k_x,\sin k_y,\sin(2k_z)]$, as illustrated in Fig. 3 and summarized in Table 4.

Table 4. Locations and topological charges of 3D meron defects in model (18).

(k_x,k_y,k_z)	$(0,0,0)$	$(0,\pi,\pi)$	$(\pi,0,\pi)$	$(\pi,\pi,0)$	$(0,\pi,\pm\frac{\pi}{2})$	$(\pi,0,\pm\frac{\pi}{2})$
Topological charge	$+1$	$+1$	$+1$	$+1$	$+1$	$+1$
(k_x,k_y,k_z)	(π,π,π)	$(0,0,\pi)$	$(0,\pi,0)$	$(\pi,0,0)$	$(0,0,\pm\frac{\pi}{2})$	$(\pi,\pi,\pm\frac{\pi}{2})$
Topological charge	-1	-1	-1	-1	-1	-1

Table 5. Contributions of topological charges to $I_{\rm N}$ and $I_{\rm S}$, as well as resultant Hopf invariants of two bands in model (18), with respect to varying m.

Locations of merons		m values						
(k_x,k_y,k_z)		$(3,+\infty)$	$(2,3)$	$(1,2)$	$(0,1)$	$(-2,0)$	$(-3,-2)$	$(-\infty,-3)$
$(0,0,0)$		$I_{\rm S}$	$I_{\rm N}$	$I_{\rm N}$	$I_{\rm N}$	$I_{\rm N}$	$I_{\rm N}$	$I_{\rm N}$
$(0,0,\pi)$,$(0,\pi,0)$,$(\pi,0,0)$		$I_{\rm S}$	$I_{\rm S}$	$I_{\rm S}$	$I_{\rm N}$	$I_{\rm N}$	$I_{\rm N}$	$I_{\rm N}$
$(0,\pi,\pi)$,$(\pi,0,\pi)$,$(\pi,\pi,0)$		$I_{\rm S}$	$I_{\rm S}$	$I_{\rm S}$	$I_{\rm S}$	$I_{\rm N}$	$I_{\rm N}$	$I_{\rm N}$
(π,π,π)		$I_{\rm S}$	$I_{\rm S}$	$I_{\rm S}$	$I_{\rm S}$	$I_{\rm S}$	$I_{\rm S}$	$I_{\rm N}$
$(0,\pi,\pm\frac{\pi}{2})$,$(\pi,0,\pm\frac{\pi}{2})$		$I_{\rm S}$	$I_{\rm S}$	$I_{\rm S}$	$I_{\rm S}$	$I_{\rm N}$	$I_{\rm N}$	$I_{\rm N}$
$(0,0,\pm\frac{\pi}{2})$		$I_{\rm S}$	$I_{\rm S}$	$I_{\rm N}$	$I_{\rm N}$	$I_{\rm N}$	$I_{\rm N}$	$I_{\rm N}$
$(\pi,\pi,\pm\frac{\pi}{2})$		$I_{\rm S}$	$I_{\rm S}$	$I_{\rm S}$	$I_{\rm S}$	$I_{\rm S}$	$I_{\rm N}$	$I_{\rm N}$
Hopf invariants	$I_{\rm N}$	0	$+1$	-1	-4	$+3$	-1	0
	$I_{\rm S}$	0	-1	$+1$	$+4$	-3	$+1$	0

Compared with Table 2, we can find eight additional merons that do not exist in model (2), which will bring extra contributions to the Hopf invariants. See Table 5 for details, where the last two rows give the Hopf invariants of the two bands. It can be easily found that $|I| > 2$ cases appear in this model.

In conclusion, we study the connection between the Hopf invariant and topological defects in the Hopf insulator, in the light of a two-band model. It is found that a 4D point defect emerges at a Dirac point, where a topological transition takes place and the Hopf invariant jumps between two distinct topological phases. For meron defects, their topological charges exactly produce the evaluations of the Hopf invariants of the two bands.

We also display an application of our theory, namely, constructing new models to realize a Hopf insulator. We propose two ways: one is to move the locations of merons; the other is to change the numbers of merons. For the latter, we present an experiential conclusion: the Hopf invariant would decrease if the number of defects reduces, while increase if the number raises.

Finally, it is noted that this study focuses on developing a new perspective to understand the Hopf invariants, which is able to provide guides for designing new Hopf insulator models. The obtained non-trivial results imply the existence of novel surface states, thanks to the bulk-boundary correspondence, which will serve as our future work.

Acknowledgements. This work was supported by the Natural Science Foundation of Beijing (Grant No. Z180007), and the National Natural Science Foundation of China (Grant Nos. 11572005 11874003, and 51672018).

References

[1] Hasan M Z and Kane C L 2010 *Rev. Mod. Phys.* **82** 3045
[2] Qi X L and Zhang S C 2011 *Rev. Mod. Phys.* **83** 1057
[3] Ando Y 2013 *J. Phys. Soc. Jpn.* **82** 102001
[4] Xu Y 2019 *Front. Phys.* **14** 43402
[5] Thouless D J, Kohmoto M, Nightingale M P, and den Nijs M 1982 *Phys. Rev. Lett.* **49** 405
[6] Qi X L, Huges T L, and Zhang S C 2008 *Phys. Rev. B* **78** 195424
[7] Chang Z W, Hao W C, and Liu X 2022 *Commun. Theor. Phys.* **74** 015701
[8] Chang Z W, Hao W C, and Liu X 2022 *J. Phys.: Condens. Matter* **34** 485502
[9] Moore J E, Ran Y, and Wen X G 2008 *Phys. Rev. Lett.* **101** 186805
[10] Deng D L, Wang S T, and Duan L M 2014 *Phys. Rev. B* **89** 075126
[11] Kennedy R 2016 *Phys. Rev. B* **94** 035137
[12] Deng D L, Wang S T, Shen C, and Duan L M 2013 *Phys. Rev. B* **88** 201105
[13] Liu C X, Vafa F, and Xu C K 2017 *Phys. Rev. B* **95** 161116
[14] Deng D L, Wang S T, Sun K, and Duan L M 2018 *Chin. Phys. Lett.* **35** 013701
[15] Schnyder A P, Ryu S, Furusaki A, and Ludwig A W W 2008 *Phys. Rev. B* **78** 195125
[16] Kitaev A 2009 *AIP Conf. Proc.* **1134** 22
[17] Wang Z, Zeng X T, Biao Y, Yan Z, and Yu R 2023 *Phys. Rev. Lett.* **130** 057201
[18] Yuan X X, He L, Wang S T, Deng D L, Wang F, Lian W Q, Wang X, Zhang C H, Zhang H L, Chang X Y, and Duan L M 2017 *Chin. Phys. Lett.* **34** 060302
[19] Yan Z B, Bi R, Shen H T, Lu L, Zhang S C, and Wang Z 2017 *Phys. Rev. B* **96** 041103
[20] Ezawa M 2017 *Phys. Rev. B* **96** 041202
[21] Bi R, Yan Z, Lu L, and Wang Z 2017 *Phys. Rev. B* **96** 201305
[22] Liu X, Zhang Y Z, Duan Y S, and Fu L B 2005 *Ann. Phys.* **318** 419